arXiv:1606.01291v1 [astro-ph.HE] 3 Jun 2016

Minimal prospects for radio detection of extensive air showers in the atmosphere of Jupiter

J. D. Bray
JBCA, School of Physics & Astronomy, University of Manchester, Manchester M13 9PL, UK
justin.bray@manchester.ac.uk

A. Nelles
Department of Physics & Astronomy, University of California, Irvine, CA 92697, USA

ABSTRACT

One possible approach for detecting ultra-high-energy cosmic rays and neutrinos is to search for radio emission from extensive air showers created when they interact in the atmosphere of Jupiter, effectively utilizing Jupiter as a particle detector. We investigate the potential of this approach. For searches with current or planned radio telescopes we find that the effective area for detection of cosmic rays is substantial ($\sim 3 \times 10^7$ km^2), but the acceptance angle is so small that the typical geometric aperture ($\sim 10^3$ km^2 sr) is less than that of existing terrestrial detectors, and cosmic rays also cannot be detected below an extremely high threshold energy ($\sim 10^{23}$ eV). The geometric aperture for neutrinos is slightly larger, and greater sensitivity can be achieved with a radio detector on a Jupiter-orbiting satellite, but in neither case is this sufficient to constitute a practical detection technique. Exploitation of the large surface area of Jupiter for detecting ultra-high-energy particles remains a long-term prospect that will require a different technique, such as orbital fluorescence detection.

Subject headings: astroparticle physics — cosmic rays — neutrinos — planets and satellites: individual (Jupiter)

1. Introduction

The spectrum of ultra-high-energy cosmic rays decreases steeply at energies above 10^{20} eV (Abraham et al. 2010). Detection of cosmic rays around and above this threshold, and potentially neutrinos at similar energies, may help to clarify whether this cut-off is due to interactions of propagating cosmic rays or an inherent limit in the spectra of their sources, to locate the positions of these sources on the sky (Abraham et al. 2007), and to determine whether there is a contribution to the cosmic-ray flux from exotic top-down mechanisms (e.g. Aloisio et al. 2015). However, detecting the rarer particles at higher energies requires detectors with extremely large apertures.

Such large apertures may potentially be obtained through remote monitoring of planet-sized bodies (Gorham 2004) such as Earth (e.g. Takahashi 2009) or the Moon (e.g. Bray et al. 2015a). As the largest body available in the solar system — apart from the Sun — Jupiter is an attractive option for this approach, and the detection of cosmic-ray interactions in its atmosphere through their gamma-ray or radio emission has been proposed (Rimmer et al. 2014) and debated (Privitera & Motloch 2014).

Codes are available to simulate the extensive air shower[1] produced when an ultra-high-energy cosmic ray or neutrino interacts in an atmosphere (Sciutto 1999), and the resulting radio emission

[1] Although "air" strictly refers to the atmosphere of Earth, we use the term "air shower" to refer to a particle cascade in any atmosphere.

(Alvarez-Muñiz et al. 2012). These codes have been validated against terrestrial air showers, and can be extended to the case of Jupiter. In this work we use these codes to analyze the development (Section 2) and radio emission (Section 3) of a Jovian air shower. In Sections 4 and 5 we examine the interaction geometry and the consequent geometric aperture for cosmic rays and neutrinos respectively, and in Section 6 we consider the prospects for detecting the radio emission from these with a realistic experiment. We discuss in Section 7 the implications of our results for the potential of Jupiter as an ultra-high-energy particle detector, and briefly summarise our conclusions in Section 8.

2. Development of Jovian air showers

When a cosmic ray interacts in the atmosphere of Jupiter, as on Earth, a shower of particles develops, generating and entraining additional particles until the energy per particle drops low enough that ionization losses dominate, and the shower dissipates. The environment on Jupiter differs from Earth in several ways which will affect the development of a shower.

- The atmosphere of Jupiter is 75% molecular hydrogen by mass, with the remainder composed almost entirely of helium. Several characteristic quantities are therefore quite different, as shown in Table 1. In particular, the radiation length is almost doubled.
- Due to the greater scale height of the Jovian atmosphere, a shower penetrating down through a given column density will develop in a less dense medium, as for showers on Earth with a large inclination angle relative to the vertical. As we shall see in Section 4, the geometry for a detectable Jovian cosmic-ray air shower requires that it be highly inclined, exacerbating this effect.
- The magnetic field of Jupiter is stronger than that of Earth, with a strength of 400 μT at the equator and 1100–1400 μT at the poles (Smith et al. 1974), versus equivalent values of 35 μT and 65 μT respectively for the geomagnetic field (Finlay et al. 2010).

To determine the effect of this differing environment on the development of an air shower, we carry out a series of simulations with the AIRES code (Sciutto 1999). AIRES has been developed to simulate showers in the terrestrial atmosphere, so to represent the Jovian atmosphere we use the TIERRAS extension (Tueros & Sciutto 2010), which allows for simulations in other media such as ice or soil. Using this extension we define a custom Jovian atmosphere, using the values for a hydrogen-helium mixture from Table 1 (except for the density, which we vary between simulations). For simplicity, in all simulations we take the primary particle to be a cosmic-ray proton. The resulting shower may differ from that produced by a neutrino, or by the heavier cosmic-ray nuclei at higher energies (Aab et al. 2014), but the radio emission is primarily determined by the energy deposited in the dominant electromagnetic component of the shower (Nelles et al. 2015), so a proton-initiated shower is an adequate model for any case with a similar shower energy.

The longitudinal development profiles of some simulated showers are shown in Figure 1, isolating the effects of each of the environmental differences listed above. The composition of the Jovian atmosphere causes the electromagnetic cascade to be elongated compared to a terrestrial shower, the reduced density suppresses the muon flux by allowing more decays, and the Jovian magnetic field, using a representative strength of 800 μT, causes the electromagnetic cascade to be strongly suppressed, as the high-energy electrons and positrons rapidly lose energy to synchrotron radiation. The synchrotron photons in this regime are high-energy gamma rays which continue to participate in the shower, but this loss still causes the shower to initially develop and attenuate more rapidly than when electrons and positrons produce gamma rays primarily through bremsstrahlung as in a classical electromagnetic cascade. This last effect, in particular, reduces the peak number of charged particles by a factor ~ 4, significantly decreasing the potential for detecting the radio emission of a Jovian air shower.

3. Radio emission from Jovian air showers

The positively and negatively charged particles in an extensive air shower, primarily electrons and positrons, are deflected in opposite directions by the local magnetic field. As electrons and

Table 1
Standard parameters for Jovian and terrestrial atmospheric gases

Composition (by mass)	Density[a] (g/cm^3)	Refractive index[a]	Radiation length (g/cm^2)	Effective Z	Mean Z/A
100% H_2	7.1×10^{-5}	1.000132	63.04	1	0.9921
100% He	12.5×10^{-5}	1.000035	94.32	2	0.4997
75% H_2/25% He[b]	8.5×10^{-5}	1.000118	68.74	1.257[c]	0.8690
terrestrial air	120.5×10^{-5}	1.000289	37.10	7.265	0.4992

[a]At standard temperature and pressure.

[b]Representative of the Jovian atmosphere.

[c]Calculated per method II of Henriksen & Baarli (1957).

References. — (Olive et al. 2014; Sciutto 1999)

positrons are continuously produced and deflected over the life of the shower, they give rise to a time-varying transverse current which is responsible for the majority of the shower radio emission. Additional emission arises from the time-varying excess of negative charge in the shower (Askaryan 1962), although this effect is usually small for showers in gaseous media. The beam pattern of the emission depends on the refractive index of the atmosphere, being enhanced at the Cherenkov angle. The basic principles of the emission mechanisms have been understood for some time (Kahn & Lerche 1966; Allan 1971), and modern microscopic simulations produce results that closely match radio observations of terrestrial air showers; see Huege (2016) for a review.

In this work we extend our simulations from Section 2 by calculating the radio emission with the ZHAireS code (Alvarez-Muñiz et al. 2012), which has been validated against observations of terrestrial air showers (e.g. Buitink et al. 2016). An additional parameter required by this code is the refractive index of the Jovian atmosphere, which we take to be

$$n_\mathrm{r} = 1 + 0.000014 \times \left(\frac{\rho}{10^{-5}\ \mathrm{g/cm^3}} \right) \qquad (1)$$

in terms of the density ρ, for non-standard temperature and pressure, based on the values in Table 1.

For an observer at the Cherenkov angle

$$\theta_\mathrm{c} = \arccos(1/n_\mathrm{r}) \qquad (2)$$

from the shower axis, the entire shower is observed near-simultaneously. Coherence over the length of the shower, and hence the amplitude of the emitted radio pulse, are therefore maximized when the observer is within a small angle $\Delta\theta$ from the Cherenkov angle. Sample pulses are shown in Figure 2, illustrating this.

To find the spectra of these pulses over frequency ν, we take their complex Fourier transform, convolve this with a variable-width window of fractional bandwidth $\Delta\nu/\nu = 0.5$, and take the magnitude of the result. This represents an observation with a corresponding experimental bandwidth, but the effect of varying this assumption is minor: for practical purposes, this is just a smoothing operation. The resulting spectra are shown in Figure 3. Depending on $\Delta\theta$, these spectra generally cut off at frequencies below a few GHz. At low frequencies, observations are limited by the background Jovian decametric radiation, with an intensity of $\sim 10^6$ Jy (Warwick 1967). This radiation cuts off sharply at a frequency of 40 MHz, corresponding to the maximum cyclotron frequency in the local magnetic field, so this may be taken as a lower limit to the frequency for practical detection of Jovian air showers.

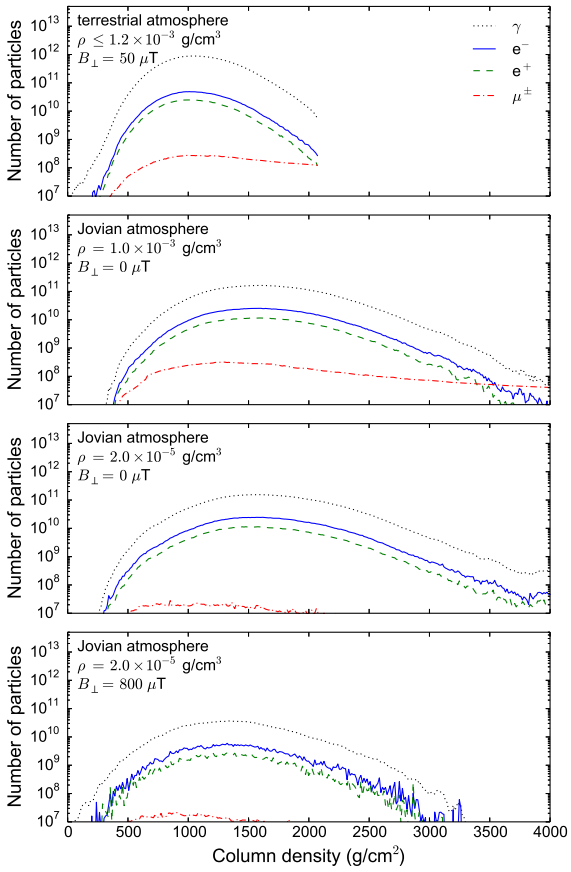

Fig. 1.— Longitudinal development of simulated air showers in terrestrial and Jovian conditions, showing the dominant particle species. The primary particle in each case is a cosmic-ray proton with an energy of 10^{20} eV. Compared to the terrestrial air shower (top), a shower in the Jovian atmosphere with comparable density ρ (upper center) develops at a greater column density because of the increased radiation length of this medium. In the less-dense upper atmosphere of Jupiter (lower center), where a detectable cosmic-ray air shower is more likely to develop (see Section 4), muons are less numerous, because the larger physical distance associated with a given column density makes them more likely to decay. The introduction of the Jovian magnetic field with a realistic transverse field strength $B_\perp$ (bottom) causes the shower to be strongly suppressed by synchrotron losses.

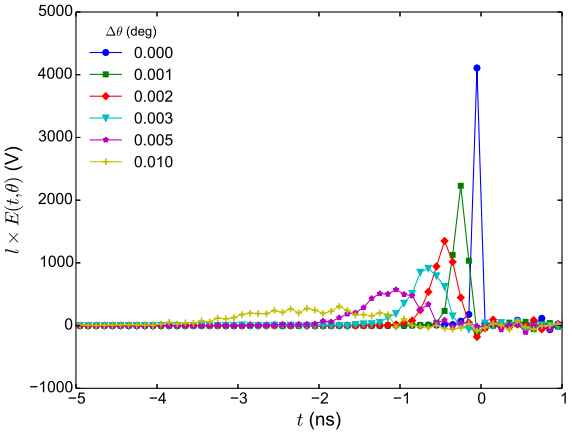

Fig. 2.— Radio pulses from a simulated Jovian air shower, showing electric field strength $E(t,\theta)$ at distance l in the far field. At greater angles $\Delta\theta$ inside the Cherenkov cone, the pulse is broader and weaker; angles outside the Cherenkov cone (not shown) display the same effect. The shower shown here had a primary cosmic-ray proton with an energy of 10^{20} eV, and developed in a Jovian atmosphere with a density of 2×10^{-5} g/cm^{-3}.

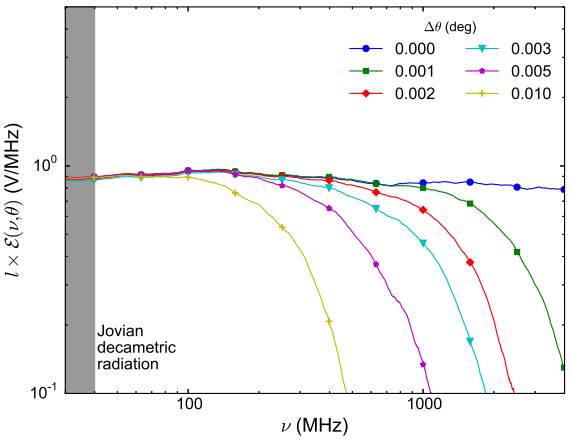

Fig. 3.— Spectra of the simulated radio pulses shown in Figure 2, showing spectral electric field strength $\mathcal{E}(\nu,\theta)$, smoothed as described in the text. At greater angles $\Delta\theta$ inside the Cherenkov cone, the pulse loses coherence and becomes weaker at higher frequencies. The shaded region shows the frequency range in which detection of the pulse is impractical because of the background Jovian decametric radiation.

The beam pattern of the emission around the Cherenkov angle, and the dependence on the energy E of the shower and the density of the medium, are shown in Figure 4. Taking a frequency-dependent Gaussian beam shape per Alvarez-Muñiz et al. (2006), and assuming a linear dependence on shower energy and a power-law dependence on density, we apply a rough parameterization of the spectral electric field as

$$\mathcal{E}(\nu,\theta;E,\rho,l) = \mathcal{E}_0 \left(\frac{E}{10^{20}\ \mathrm{eV}}\right)\left(\frac{\rho}{10^{-5}\ \mathrm{g/cm^3}}\right)^{\alpha} \times \left(\frac{l}{8\times10^{11}\ \mathrm{m}}\right)^{-1} \exp\left(-\left(\frac{\Delta\theta}{\theta_c}\right)^2\left(\frac{\nu}{\nu_0}\right)^2\right) \quad (3)$$

where $l = 8\times10^{11}$ m is the mean distance from Earth to Jupiter. For the free parameters in this expression we fit the values

$$\mathcal{E}_0 = 5.7\times10^{-7}\ \mu\mathrm{V/m/MHz} \quad (4)$$

$$\nu_0 = 6.9\ \mathrm{MHz} \quad (5)$$

$$\alpha = 0.94 \quad (6)$$

using a series of simulations spanning the ranges 10^{19} eV to 10^{21} eV in energy and 1×10^{-5} g/cm^3 to 5×10^{-5} g/cm^3 in density. To test the accuracy of these values, we simulate a single additional shower, and compare its radio emission with that predicted by the parameterization. We find that the parameterization predicts the width of the emission beam in the angular variable $\Delta\theta$ to within a factor of two, which will determine the resulting error in the geometric apertures calculated in Sections 4 and 5. We expect the linear dependence on E in Equation 3 to hold reasonably well outside the energy range used for our fit, as this linearity is a consistent feature of coherent pulses from particle cascades.

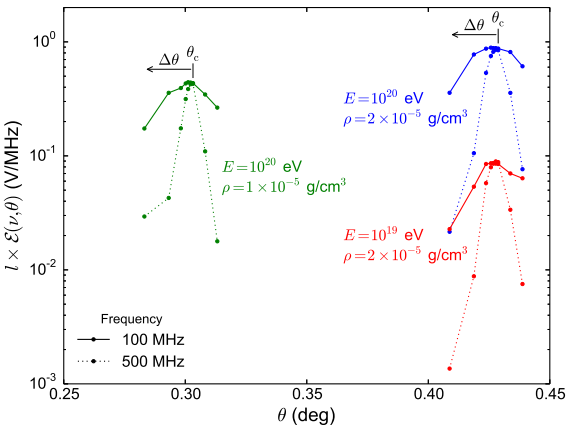

Fig. 4.— Beam patterns of radio pulses from simulated Jovian air showers, showing spectral electric field strength $\mathcal{E}(\nu,\theta)$ at distance l in the far field. The radiation is beamed as a hollow cone at the Cherenkov angle $\theta = \theta_c$ from the axis of the shower. If the shower develops at a lower atmospheric density (left; green), then the emission is weaker than for a similar shower at a higher density (top-right; blue), and the Cherenkov angle is smaller. If the shower has a lower energy (bottom-right; red), the emission is weaker but the Cherenkov angle is unchanged. In all cases, the radiation has a smaller beam width scale $\Delta\theta$ at higher frequencies.

4. Geometric aperture for cosmic rays

For a cosmic ray interacting in the Jovian atmosphere to be detected, it must meet two conditions: the interaction must be sufficiently deep that the extensive air shower will fully develop and produce coherent radio emission, and sufficiently shallow that this radio emission — directed forward along the axis of the shower — is not completely attenuated as it escapes the atmosphere. These conditions constrain detectable cosmic rays to trajectories that skim the atmosphere of Jupiter, as

described by Rimmer et al. (2014) and illustrated in Figure 5. The detection region is an annulus around Jupiter with a width of ΔR and a circumference of $2\pi R_{\rm J}$, where $R_{\rm J} = 6.9 \times 10^4$ km is the mean radius of Jupiter.

For the full development of an air shower, we require that the total column density $X_{\rm tot}$ of the Jovian atmosphere along its path is sufficient for it to reach its point of maximum development, at a column depth of $X_{\rm max} \sim 1500$ g/cm^2. We calculate $X_{\rm tot}$ from the atmospheric density profile of Moses et al. (2005), similarly to Rimmer et al. (2014), and find the altitude of the lowest point on the axis of the air shower for which $X_{\rm tot} > X_{\rm max}$, as shown in Figure 6. This is not a precise limit, as showers above this altitude will have non-zero radio emission, and showers slightly below this altitude will have reduced radio emission due to their truncation soon after their point of maximum development. However, due to the exponential profile of the atmosphere, modifying this assumption will have a relatively small effect on the maximum altitude $R_{\rm max}$ of the detection region.

For the radio emission to escape, we require that the projected shower axis pass no deeper than a pressure of 1000 mbar, at which Lindal et al. (1981) found the S-band signal from the Voyager 1 probe at 2.3 GHz to be extinguished due to absorption by ammonia. This condition implies that the radio emission is assumed to be unattenuated up to a radio attenuation length of $X_{\rm att,r} = 6 \times 10^4$ g/cm^2, calculated from the model of Moses et al. (2005) as above, and completely attenuated beyond this threshold. This is around an order of magnitude larger than the attenuation length we calculate from measurements with the Galileo probe (Folkner et al. 1998), and from the model of Janssen et al. (2005), but these results are for near-vertical transects, and are therefore more sensitive to conditions at low altitudes, with a greater relative concentration of radio-absorbing ammonia. As the Jupiter-skimming geometry of the Voyager measurement better represents the air-shower geometry considered in this work, we will use the larger number for the radio attenuation length, and acknowledge that it may lead to an optimistic value for the cosmic-ray aperture. We also neglect the frequency dependence of the radio attenuation; but, as for $R_{\rm max}$ above, the exponential profile of the atmosphere will restrict

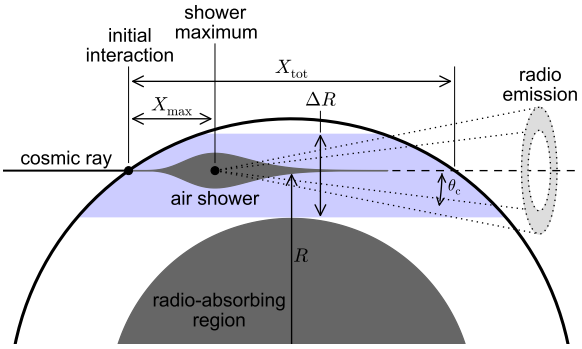

Fig. 5.— Interaction geometry for a detectable Jovian air shower. The shower develops from the initial interaction, reaching its maximum development at a column depth $X_{\rm max} \sim 1500$ g/cm^2. The radio emission from the shower is beamed forward as a hollow cone at the Cherenkov angle $\theta_{\rm c}$ around the projected shower axis (dashed). For the shower to be detectable, it must be sufficiently deep that the total column density $X_{\rm tot} > X_{\rm max}$ allows it to completely develop, but not so deep that the radio emission is absorbed.

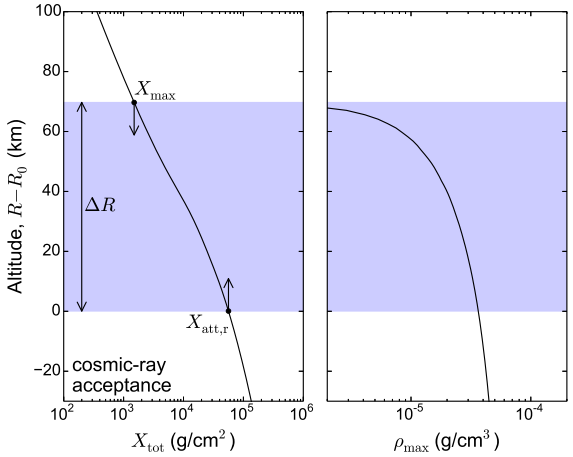

Fig. 6.— Range of altitudes (shaded) for the lowest point on the projected path of a detectable cosmic ray through the Jovian atmosphere, at radius R as illustrated in Figure 5. As shown in the left panel, we require that the column density $X_{\rm tot}$ along the path of the cosmic ray be at least $X_{\rm max} \sim 1500$ g/cm^2, and no greater than the radio attenuation length $X_{\rm att,r}$. The right panel shows $\rho_{\rm max}$, the density at a column depth of $X_{\rm max}$, at which the shower development is maximized. The reference zero altitude, at radius R_0, is at a pressure of 1000 mbar.

these approximations to a relatively small effect on the minimum altitude $R_{\min}$ of the detection region.

Between the altitudes $R_{\min}$ and $R_{\max}$ we find a range of $\Delta R = 70$ km as shown in Figure 6. The resulting area of the annular detection region is $2\pi R_{\rm J} \Delta R = 3 \times 10^7$ km^2, which is substantial: it exceeds the area of the Pierre Auger Observatory (Aab et al. 2015b), the largest current cosmic-ray detector, by four orders of magnitude. However, a cosmic ray passing through this area will only be detected if its beamed emission is directed towards a radio antenna. The resulting acceptance angle for a detectable cosmic ray, assuming a single radio antenna (e.g. at Earth), has the same solid angle as the emission, or

$$\Omega = 4\pi\, \theta_{\rm c}\, \Delta\theta_{\max} \tag{7}$$

where $\Delta\theta_{\max}$ is the maximum separation from the Cherenkov angle at which the pulse can be detected. For a typical Cherenkov angle and beam scale width of $\theta_{\rm c} \sim 0.4^\circ$ and $\Delta\theta_{\max} \sim 0.02^\circ$ respectively (see Figure 4), this results in a geometric aperture of $2\pi R_{\rm J} \Delta R\, \Omega \sim 10^3$ km^2 sr, which is less than those of current detectors.

More generally, we can find the geometric aperture as

$$A(E; \mathcal{E}_{\rm thr}) = \int_{R_{\min}}^{R_{\max}} 2\pi R_{\rm J}\, dR\; \Omega(\mathcal{E}_{\rm thr}) \tag{8}$$

where $\Omega(\mathcal{E}_{\rm thr})$ is the solid angle in which the pulse amplitude exceeds a detection threshold of $\mathcal{E}_{\rm thr}$, which describes the radio sensitivity of a coherent pulse detection experiment. To calculate $\Omega(\mathcal{E}_{\rm thr})$, we first solve Equation 3 for $\Delta\theta$ with $\mathcal{E} = \mathcal{E}_{\rm thr}$, and then use this value as $\Delta\theta_{\max}$ when calculating Ω from Equation 7. We assume in Equation 3 that $\rho = \rho_{\max}$ is evaluated at a column depth of $X_{\max} = 1500$ g/cm^2 along the shower axis, effectively assuming that the entire cascade occurs in a medium corresponding to the density at the shower maximum. Across the altitude range ΔR, these densities take values up to a maximum of 3.6×10^{-5} g/cm^3, falling within the parameter range of our simulations in Section 3. Some sample apertures for idealized Earth-based radio antennas are shown in Figure 7. In Section 6, we consider the prospects of detecting cosmic rays with some realistic experiments.

5. Geometric aperture for neutrinos

Neutrinos differ from cosmic rays in that they are able to propagate through a substantial depth of Jovian atmosphere before they interact and initiate an air shower. However, ultra-high-energy neutrinos are still unable to propagate directly through the bulk of Jupiter, so detectable neutrinos are also constrained to trajectories that skim its atmosphere, albeit at greater depths than cosmic rays, as illustrated in figure 8. Since the radio attenuation length $X_{\rm att,r}$ is substantially smaller than the neutrino attenuation length $X_{{\rm att},\nu}$, the majority of interacting neutrinos will produce air showers too deep in the atmosphere for the radio emission to escape. As in Section 4, we will assume the radio emission from an air shower to escape if it propagates through a column density less than $X_{\rm att,r}$, and to be completely attenuated otherwise.

The deepest possible path for a detectable neutrino is determined by neutrino absorption in the lower atmosphere. This regime lies beyond that described by the atmospheric model of Moses et al. (2005) used in Section 4, so we extend it to lower altitudes using measurements from the Galileo mission (Seiff et al. 1998), and extrapolate still further assuming a constant scale height (see Figure 9). As shown in Figure 10, we require that the total column density $X_{\rm tot}$ along the path of the neutrino be less than the neutrino attenuation length $X_{{\rm att},\nu}$, which we find from the neutrino interaction cross-sections modeled by Block et al. (2010), with a power-law extrapolation to higher energies (see Figure 11). This is an approximation, assuming that neutrinos experience no attenuation at less than a single attenuation length, and are completely attenuated beyond this threshold, as well as neglecting the recycling of interacting neutrinos to lower energies, which causes a factor ~ 1.4 increase in the neutrino flux (Gayley et al. 2009). However, as in Section 4, modifying this assumption will have a relatively small effect on the minimum altitude $R_{\min}$ of the detection region.

For a neutrino to be detected, it must interact in the final radio attenuation length $X_{\rm att,r}$ along the total column density $X_{\rm tot}$, so the radio emission from the resulting air shower can escape. If the neutrino follows a shallow path through the atmosphere, such that $X_{\rm tot} < X_{\rm att,r}$, it is proportionately less likely to interact. As shown in Fig-

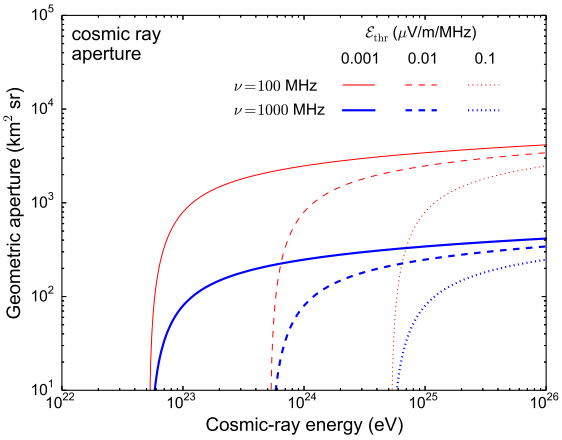

Fig. 7.— Geometric apertures of Earth-based radio antennas for the detection of cosmic rays interacting in the atmosphere of Jupiter. The minimum detectable cosmic-ray energy is determined by the radio detection threshold $\mathcal{E}_{\rm thr}$, and the maximum geometric aperture is determined by the observing frequency ν.

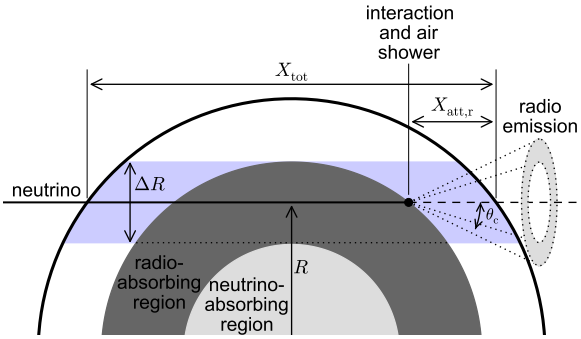

Fig. 8.— Interaction geometry for a detectable Jovian air shower initiated by a neutrino (cf. figure 5). For the neutrino to be detectable, it must interact on its way out of the planet, with the remaining atmospheric column density along its path less than the radio attenuation length $X_{\rm att,r}$, so radio emission can escape from the resulting air shower (which has a length scale $X_{\rm max} \ll X_{\rm att,r}$). This implies that the path of the neutrino should be sufficiently deep that the total column density $X_{\rm tot} \gtrsim X_{\rm att,r}$, so there is an appreciable chance that the neutrino will interact, but not so deep that $X_{\rm tot}$ exceeds the neutrino attenuation length $X_{{\rm att},\nu}$, in which case it is likely to be absorbed deep within the planet.

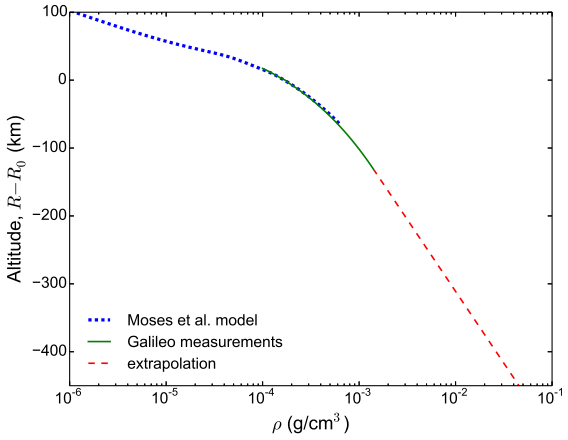

Fig. 9.— Density profiles for the atmosphere of Jupiter used in this work: from the model of Moses et al. (2005), from measurements by the Galileo probe (Seiff et al. 1998), and an extrapolation of the latter with a constant scale height of 92 km.

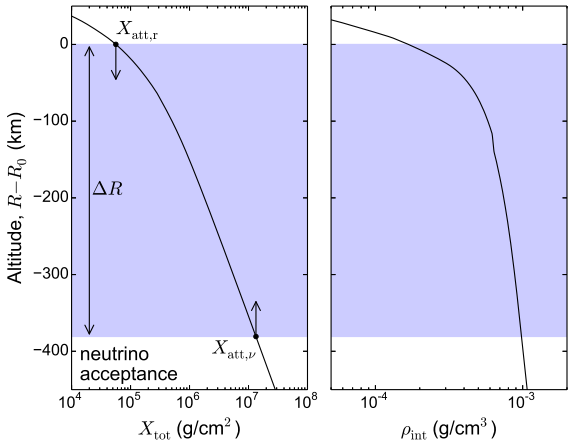

Fig. 10.— Range of altitudes (shaded) for the lowest point on the path of a detectable neutrino through the Jovian atmosphere, at radius R as illustrated in Figure 8. As shown in the left panel, we require that the column density $X_{\rm tot}$ along the path of the neutrino is greater than the radio attenuation length $X_{\rm att,r}$ and lesser than the neutrino attenuation length $X_{{\rm att},\nu}$. This latter bound is slightly energy-dependent; the limit shown here is for $E_\nu = 10^{23}$ eV. The right panel shows $\rho_{\rm int}$, the maximum density along the projected neutrino path within $X_{\rm att,r}$ of the exit point; this represents the point at which a detectable air shower is most likely to occur.

ure 8, we neglect this reduced probability of interaction, taking the maximum altitude $R_{\max}$ of the detection region to be defined by the limit $X_{\rm tot} = X_{\rm att,r}$. Neglecting those neutrinos that interact on shallower trajectories than this will cause us to underestimate the neutrino aperture, but this is a relatively small effect, both because these interactions are less common and because those air showers that do develop will do so in a less dense medium, and hence produce less radio emission.

Given these approximations, we can find the neutrino aperture similarly to Equation 8, as

$$A(E_\nu; \mathcal{E}_{\rm thr}) = \frac{X_{\rm att,r}}{X_{\rm att,\nu}} \int_{R_{\min}}^{R_{\max}} 2\pi R_{\rm J}\, dR\ \Omega(\mathcal{E}_{\rm thr}) \quad (9)$$

where the initial ratio $X_{\rm att,r}/X_{\rm att,\nu} \sim 10^{-2}$ represents the probability of the neutrino interacting within one radio attenuation length of the exit point. In calculating $\Omega(\mathcal{E}_{\rm thr})$ here we assume that the shower develops in a medium with a density $\rho = \rho_{\max}$, the maximum atmospheric density along this final segment of the neutrino path, as shown in Figure 10; note that these values are typically around 10^{-3} g/cm^3, so we are extrapolating outside the range of our simulations in Section 3. In practice ρ may take any value from $\rho_{\max}$ down to a minimum of near-zero density, for a neutrino that interacts in the outer reaches of the Jovian atmosphere, but the initial interaction is more likely to occur in a high-density region, hence our assumption. We also assume that the shower energy is 20% of the neutrino energy E_ν, typical for the hadronic shower from a neutrino-nucleon interaction (James & Protheroe 2009).

In Figure 12 we show some sample neutrino apertures for the same idealized Earth-based radio antennas as for cosmic rays in Figure 7. Compared to the case for cosmic rays, we might expect that the aperture would be reduced, due to the low probability that a neutrino will interact high enough in the atmosphere for the radio emission to escape, and that the energy threshold would be increased, as only a fraction of the original particle energy is manifested in the air shower. However, air showers initiated by neutrinos typically begin deeper in the atmosphere and hence develop in a denser medium (see Figures 6 and 10), which counteracts both of these effects: per Equation 3, air showers developing in a denser medium will have stronger emission, allowing less-energetic showers to be detected; and the emission will be beamed at a larger Cherenkov angle, increasing the solid angle of the emission. The net effect is that the aperture for detection of neutrinos is slightly larger than that for cosmic rays, and the energy threshold is slightly lower. In Section 6, we will examine how these apertures translate into prospects of detecting neutrinos with some realistic experiments.

6. Detection prospects

To date, the experiment with the greatest sensitivity to coherent astronomical pulses is the LUNASKA Parkes experiment (Bray et al. 2015a), which used the Parkes radio telescope to search for pulses from particle cascades in the lunar regolith. The most sensitive future radio telescope currently being developed, Phase 1 of the Square Kilometre Array (SKA), will have substantially greater sensitivity in the same role (Bray et al. 2015b). If these telescopes were used instead to search for radio pulses from Jupiter, they would constitute experiments capable in principle of detecting Jovian air showers, albeit with some technical challenges such as compensating for dispersion of the pulse in the Jovian ionosphere. Parameters for these experiments are listed in Table 2.

Another possibility is to search for radio pulses using an antenna on a Jupiter-orbiting satellite, which has the advantage of closer proximity to the source of the pulse. To explore the potential of this approach, we consider a hypothetical satellite experiment with a radio collecting area of 100 m^2, and 100 MHz of bandwidth centered on an observing frequency of $\nu = 100$ MHz, close to the minimum-frequency limit imposed by the Jovian decametric radiation, to maximize the aperture. The system noise at this frequency will be dominated by received radiation, from both Jupiter and the background sky; at this frequency the brightness temperature of the Galactic synchrotron background is ~ 1000 K (Thompson et al. 2001), and the atmosphere of Jupiter is transparent down to an altitude with a similar temperature (Janssen et al. 2005), so we take this value as the system temperature. The noise level can then be calculated as $\mathcal{E}_{\rm rms} = 0.023$ μV/m/MHz (Bray 2016, Equation 7), and the threshold for a confident detection may reasonably be taken to be ten times this value. The particle aperture will

TABLE 2
POTENTIAL SENSITIVITY OF COHERENT PULSE DETECTION EXPERIMENTS

Experiment	Threshold ($\mathcal{E}_{\rm thr}/(\mu$V/m/MHz))	Frequency (ν/MHz)	Distance (l/m)	Observing time ($t_{\rm obs}$/h)
LUNASKA Parkes[a]	0.0047	1350	8×10^{11}	127.2
SKA-lunar[a]	0.0014	225	8×10^{11}	1000
satellite (high altitude)	0.23	100	2.4×10^{7}	8760
satellite (low altitude)	0.23	100	1.2×10^{8}	8760

[a]These experiments are/were not designed to detect Jovian air showers. These parameters reflect their potential sensitivity if they had been so designed.

References. — (Bray et al. 2015a,b)

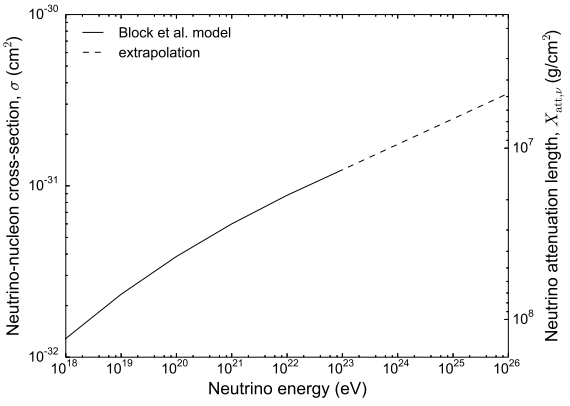

Fig. 11.— Total neutrino-nucleon interaction cross-section σ from Block et al. (2010) (solid) and a power-law extrapolation to higher energies (dashed). The corresponding column density for neutrino attenuation is shown on the right axis, found as $X_{{\rm att},\nu} = m_{\rm n}/\sigma$ where $m_{\rm n}$ is the nucleon mass.

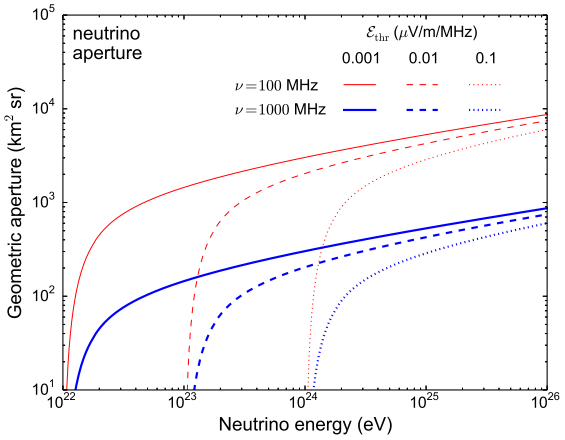

Fig. 12.— Geometric apertures of Earth-based radio antennas for the detection of neutrinos interacting in the atmosphere of Jupiter, for different radio detection thresholds $\mathcal{E}_{\rm thr}$ and observing frequencies ν. The apertures are generally larger, and the energy thresholds generally lower, than those shown for cosmic rays in Figure 7.

depend on the altitude of the satellite (see Figure 13), with a satellite closer to the planet being sensitive to less-energetic particles, but viewing a smaller volume of atmosphere. We consider two scenarios with the satellite at altitudes of $h = 4000$ km, corresponding to the minimum perijove for the Juno probe (Janssen et al. 2014), and $h = R_{\rm J} = 69000$ km, and assume that in either scenario the satellite could be operated for a period of one year. Parameters for these experiments are also listed in Table 2.

Note that this hypothetical satellite is optimistic compared to practical near-future instruments. The collecting area and bandwidth are comparable to the existing space radio telescope RadioAstron (Kardashev et al. 2013), but this instrument is in Earth orbit, not subject to the challenges of deployment to Jupiter or survival in the harsh Jovian environment, particularly its intense radiation belts. The most sensitive radio instrument to be deployed this close to Jupiter is the microwave radiometer on the Juno probe (Janssen et al. 2014), the largest antenna of which has an area of ~ 2 m^2 and a bandwidth of 21 MHz, substantially less than assumed here. Furthermore, a single antenna beam does not have a sufficient field of view to view the entire horizon of Jupiter as required in this application; our hypothetical satellite would require multiple antennas or a phased array, with concomitant signal-processing requirements.

We calculate the apertures of the Earth-based experiments for the detection of cosmic rays and neutrinos with Equations 8 and 9 respectively. For the satellite experiments, we do the same, but replace the $2\pi R_{\rm J}$ factor for the circumference of Jupiter with $2\pi r$ for the circumference of the visible horizon (see Figure 13). In both cases, we find the projected differential limits on the cosmic-ray or neutrino flux as

$$\frac{dF}{dE} < \frac{2.3}{EA(E)\,t_{\rm obs}} \qquad (10)$$

where $t_{\rm obs}$ is the total observing time and the factor of 2.3 comes from the Poissonian distribution of the expected number of events for a 90%-confidence limit. These projected limits are shown for cosmic rays and neutrinos in Figures 14 and 15 respectively.

The projected cosmic-ray limits, shown in Figure 14, do not extend down to sufficiently low energies to detect the known cosmic-ray flux. Their energy range is suitable for testing predicted cosmic-ray fluxes from exotic top-down mechanisms, such as the decay of super-heavy dark matter (Aloisio et al. 2015); models of this class are generally constrained by limits on the fluxes of ultra-high-energy neutrinos (Gorham et al. 2010) and photons (Abraham et al. 2009), but not entirely ruled out. However, even these speculative fluxes are too low to be detected: the satellite experiments would need to be more sensitive by two orders of magnitude, while the experiments with Earth-based radio telescopes, LUNASKA Parkes and SKA-lunar, have even worse prospects.

The projected limits for neutrinos, shown in Figure 15, are slightly more promising. The Earth-based experiments are still unable to detect the neutrino fluxes predicted from top-down mechanisms, but the satellite experiments are able to test some of the more optimistic models in this class. The low-altitude satellite experiment has substantially better performance than its high-altitude equivalent, and is almost capable of detecting the cosmogenic neutrino flux expected from photopion interactions of propagating cosmic rays, regardless of the cosmic-ray origin model (Kotera et al. 2010). However, there are several projects under development, including ARA (Allison et al. 2012) and ARIANNA (Barwick et al. 2015), that are likely to detect the cosmogenic neutrino flux in the near future, with substantially less risk and expense than a Jupiter-orbiting satellite.

7. Discussion

The prospect of utilizing Jupiter with its 6×10^{10} km^2 of surface area as a detector for cosmic rays or neutrinos is an attractive one. The only larger body in the solar system, the Sun, is a strong source of background radiation that makes it highly impractical to use in this role. Consequently, no larger particle aperture than that of Jupiter will be available for the foreseeable future.

However, searches for radio emission from Jovian air showers are not a practical means of exploiting Jupiter as a particle detector. We have found in this work that, with current or planned Earth-based radio telescopes, this technique is sen-

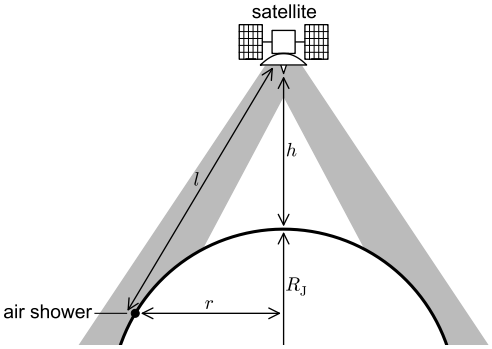

Fig. 13.— Geometry for radio air-shower detection with a Jupiter-orbiting satellite. The antenna beams (shaded) must observe around the limb of the planet, so as to detect air showers in the atmosphere-skimming geometries shown in Figures 5 and 8. If the altitude h of the satellite is decreased, there is a shorter distance l to the air shower, allowing a less energetic shower to be detected. However, the circumference $2\pi r$ of the horizon viewed by the satellite is also decreased, leading to a reduced aperture for cosmic rays or neutrinos.

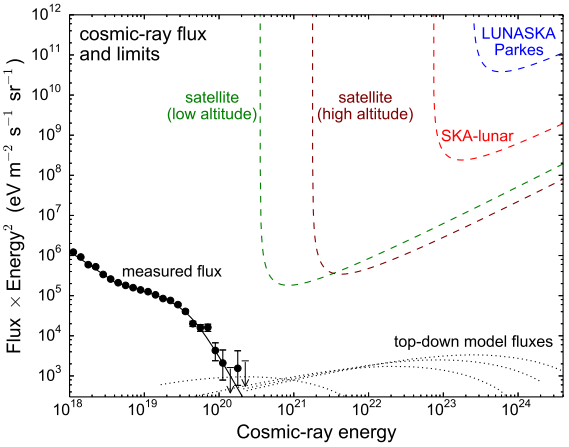

Fig. 14.— Ultra-high-energy cosmic-ray flux and potential limits from radio observations of Jupiter. The points and solid line show the measured cosmic-ray flux and fit (Abraham et al. 2010), while dotted lines show speculative cosmic-ray proton fluxes from decay of super-heavy dark matter (Aloisio et al. 2015). Dashed lines show potential limits from radio searches for Jovian air showers with the experiments described in the text.

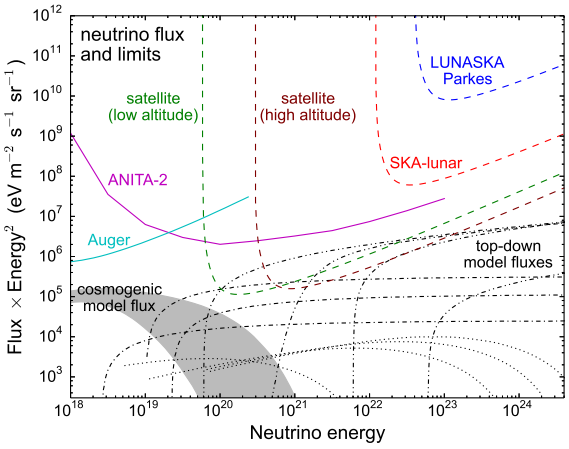

Fig. 15.— Models of the ultra-high-energy neutrino flux, existing limits, and potential limits from radio observations of Jupiter. The shaded region shows a range of models for the expected cosmogenic neutrino flux (Kotera et al. 2010), while more speculative models for neutrinos from various top-down mechanisms are shown from Aloisio et al. (2015), dotted; Berezinsky et al. (2011), dash-dotted; and Lunardini & Sabancilar (2012), dash-dot-dotted. Solid lines show limits established by the ANITA experiment (Gorham et al. 2010) and the Pierre Auger Observatory (Aab et al. 2015a) under the same definition as in Equation 10. Dashed lines show potential limits from radio searches for Jovian air showers with the experiments described in the text.

sitive only to cosmic rays above an extremely high energy threshold, $\sim 10^{23}$ eV, and even then only to fluxes orders of magnitude higher than the most optimistic predictions in this energy range. The situation with respect to neutrinos is similar. A hypothetical highly-capable radio detector in close orbit around Jupiter might be able to test some of the more optimistic models of the neutrino flux, but this is a poor return for such a challenging experiment.

Our results here are not precise — we have, for example, inaccuracy of a factor ~ 2 in our parameterization of the radio emission from a shower — but a more precise analysis is unlikely to be so much more optimistic than this work that it predicts this technique to be practical. Our most serious approximation is probably our simplistic model of radio attenuation, which could be improved by implementing a radiative transfer model such as that of Janssen et al. (2005), but our assumptions err on the side of optimism, and a more sophisticated analysis is most likely to revise the sensitivity substantially downwards.

Our results conflict with those of Rimmer et al. (2014), who found that it was practical to detect radio emission from Jovian air showers with present-day instruments. However, Rimmer et al. developed their own model of the radio emission in which it is represented as classical synchrotron radiation, which has proven to be a poor approximation to real air showers (Huege 2016, Section 3.1). As the ZHAireS code used in this work has been validated against observations of terrestrial air showers, we expect our results to be more reliable.

The major effect identified in this work is that, for the forward-beamed radio emission from a shower to escape Jupiter, the shower must be inclined almost horizontally, which causes it to develop in the upper atmosphere where the density is low. In this environment, the radio emission is very narrowly beamed, which leads to a small cosmic-ray acceptance angle and hence a small geometric aperture. This effect is less pronounced for neutrinos, which are able to pass more deeply through the planet and interact in the lower atmosphere on a trajectory that is inclined slightly upward. Consequently, the aperture for neutrinos is larger than that for cosmic rays, though not sufficiently so to make detection practical.

We expect similar results to apply for the other gas giant planets in the solar system. Each of them has a radius smaller than that of Jupiter, which allows a horizontally-inclined shower to develop at a lower altitude, but each also has a lower surface gravity and hence a larger atmospheric scale height, so the density at a given altitude will be reduced; combined, these effects may cause the typical density under which an air shower develops, and hence also the strength of its radio emission, to increase or decrease slightly. The magnetic fields of the other gas giants are also weaker than the ~ 800 μT field of Jupiter (e.g. Saturn, 21 μT; Davis & Smith 1990), which will reduce the strength of radio emission from showers in their atmospheres, though it will also ameliorate the shower suppression due to synchrotron losses. Finally, all of the other gas giants are more distant than Jupiter, reducing the effectiveness of Earth-based instruments.

Our results also apply to other forms of radiation emitted by a Jovian air shower, provided that they are beamed at the Cherenkov angle and do not penetrate the lower atmosphere of Jupiter more efficiently than radio. Optical Cherenkov radiation meets these conditions, and so is also excluded as a practical means of detecting Jovian air showers.

Our results do not exclude the possibility of practical detection of Jovian air showers through an emission mechanism that radiates isotropically, such as atmospheric fluorescence. Orbital detection of atmospheric fluorescence from terrestrial air showers in the 330–400 nm band is being pursued by the JEM-EUSO project (Takahashi 2009), and the same technique could be applied with an imaging telescope in orbit around Jupiter. The depth at which an air shower can be detected will be limited by Rayleigh scattering, for which an optical depth of unity for the JEM-EUSO band is reached in the Jovian atmosphere at a pressure of ~ 2000 mbar (West et al. 2004, Figure 5.3), slightly deeper than the minimum altitude found in this work for radio detection of cosmic rays. However, the JEM-EUSO band is tuned to the fluorescence spectrum of nitrogen, which is almost non-existent in the Jovian atmosphere. Molecular hydrogen fluoresces primarily at wavelengths < 200 nm (Sternberg 1989), which are much more strongly affected by Rayleigh scattering; better

results may be obtained with the helium line at 502 nm (Becker et al. 2010), although helium is a minor constituent ($\sim 25\%$ by mass) of the Jovian atmosphere.

8. Summary

We have investigated the potential for detecting radio emission from extensive air showers initiated in the atmosphere of Jupiter by ultra-high-energy cosmic rays or neutrinos. We have developed models for the geometry under which such showers might be detected, simulated their development under representative Jovian conditions, and compared the strength of their radio emission to the sensitivity of current and planned Earth-based radio telescopes, and of a hypothetical radio detector in Jovian orbit.

We find that none of our considered experiments are likely to detect air showers initiated by cosmic rays, nor are Earth-based instruments likely to detect air showers initiated by neutrinos. Under generous assumptions, a Jupiter-orbiting satellite may be able to detect some of the more optimistic predictions of the ultra-high-energy neutrino flux.

Our findings indicate that radio detection is unlikely to be a practical means to exploit the aperture of Jupiter as a particle detector. Orbital fluorescence detection remains a possibility: its application to Jupiter seems to offer no compelling advantages, but may become worthwhile at some point in the future if the aperture provided by the Earth is fully exploited.

The authors would like to thank Jaime Alvarez-Muñiz and Washington Carvalho Jr. for helpful discussions concerning ZHAireS, and an anonymous referee for several helpful comments regarding the content of the manuscript. JDB acknowledges support from ERC-StG 307215 (LODESTONE). AN is supported by the DFG (research fellowship NE 2031/1-1).

REFERENCES

Aab, A., Abreu, P., Aglietta, M., et al. 2014, Phys. Rev. D, 90, 122006

—. 2015a, Phys. Rev. D, 91, 092008

—. 2015b, Nucl. Instrum. Meth. A, 798, 172

Abraham, J., Abreu, P., Aglietta, M., et al. 2007, Science, 318, 938

—. 2009, Astropart. Phys., 31, 399

—. 2010, Phys. Lett. B, 685, 239

Allan, H. R. 1971, in Progress in Elementary Particle and Cosmic Ray Physics, Vol. 10, Progress in Elementary Particle and Cosmic Ray Physics, ed. J. G. Wilson & S. A. Wouthuysen (Amsterdam/London: North-Holland), 171–302

Allison, P., Auffenberg, J., Bard, R., et al. 2012, Astropart. Phys., 35, 457

Aloisio, R., Matarrese, S., & Olinto, A. V. 2015, J. Cosmology Astropart. Phys., 8, 24

Alvarez-Muñiz, J., Carvalho, W. R., Tueros, M., & Zas, E. 2012, Astropart. Phys., 35, 287

Alvarez-Muñiz, J., Marqués, E., Vázquez, R. A., & Zas, E. 2006, Phys. Rev. D, 74, 023007

Askaryan, G. A. 1962, Sov. Phys. JETP, 14, 441

Barwick, S. W., Berg, E. C., Besson, D. Z., et al. 2015, Astropart. Phys., 70, 12

Becker, F., Forck, P., Giacomini, T., Haseitl, R., & Walasek-Hoehne, B. 2010, in Proc. 14th Beam Instrumentation Workshop, Joint Accelerator Conferences Website, 156–159

Berezinsky, V., Sabancilar, E., & Vilenkin, A. 2011, Phys. Rev. D, 84, 085006

Block, M. M., Ha, P., & McKay, D. W. 2010, Phys. Rev. D, 82, 077302

Bray, J. 2016, Astropart. Phys., 77, 1

Bray, J. D., Ekers, R. D., Roberts, P., et al. 2015a, Astropart. Phys., 65, 22

Bray, J. D., Alvarez-Muñiz, J., Buitink, S., et al. 2015b, in Proc. Sci., Vol. 215, Advancing Astrophysics with the Square Kilometre Array, 144

Buitink, S., Corstanje, A., Falcke, H., et al. 2016, Nature, 531, 70

Davis, Jr., L., & Smith, E. J. 1990, J. Geophys. Res., 95, 15257

Finlay, C. C., Maus, S., Beggan, C. D., et al. 2010, Geophys. J. Int'l, 183, 1216

Folkner, W. M., Woo, R., & Nandi, S. 1998, J. Geophys. Res., 103, 22847

Gayley, K. G., Mutel, R. L., & Jaeger, T. R. 2009, ApJ, 706, 1556

Gorham, P. W. 2004, Planet-sized Detectors for Ultra-high Energy Neutrinos & Cosmic Rays, Capability roadmap, NASA Advanced Planning Office, arXiv:astro-ph/0411510

Gorham, P. W., Allison, P., Baughman, B. M., et al. 2010, Phys. Rev. D, 82, 022004

Henriksen, T., & Baarli, J. 1957, Radiation Res., 6, 415

Huege, T. 2016, Phys. Rep., 620, 1

James, C. W., & Protheroe, R. J. 2009, Astropart. Phys., 30, 318

Janssen, M. A., Brown, S. T., Oswald, J. E., & Kitiyakara, A. 2014, in Proc. IRMMW-THz 2014

Janssen, M. A., Hofstadter, M. D., Gulkis, S., et al. 2005, Icarus, 173, 447

Kahn, F. D., & Lerche, I. 1966, Proc. R. Soc. A, 289, 206

Kardashev, N. S., Khartov, V. V., Abramov, V. V., et al. 2013, Astron. Rep., 57, 153

Kotera, K., Allard, D., & Olinto, A. V. 2010, J. Cosmology Astropart. Phys., 10, 13

Lindal, G. F., Wood, G. E., Levy, G. S., et al. 1981, J. Geophys. Res., 86, 8721

Lunardini, C., & Sabancilar, E. 2012, Phys. Rev. D, 86, 085008

Moses, J. I., Fouchet, T., Bézard, B., et al. 2005, J. Geophys. Res., 110, 8001

Nelles, A., Buitink, S., Falcke, H., et al. 2015, Astropart. Phys., 60, 13

Olive, K. A., Agashe, K., Amsler, C., et al. 2014, Chinese Phys. C, 38, 090001

Privitera, P., & Motloch, P. 2014, ApJ, 791, L15

Rimmer, P. B., Stark, C. R., & Helling, C. 2014, ApJ, 787, L25

Sciutto, S. J. 1999, AIRES: A system for air shower simulations, Tech. rep., Pierre Auger Collaboration, arXiv:astro-ph/9911331

Seiff, A., Kirk, D. B., Knight, T. C. D., et al. 1998, J. Geophys. Res., 103, 22857

Smith, E. J., Davis, Jr., L., Jones, D. E., et al. 1974, J. Geophys. Res., 79, 3501

Sternberg, A. 1989, ApJ, 347, 863

Takahashi, Y. 2009, New J. Phys., 11, 065009

Thompson, A. R., Moran, J. M., & Swenson, Jr, G. W. 2001, Interferometry and Synthesis in Radio Astronomy, 2nd edn. (Wiley-VCH)

Tueros, M., & Sciutto, S. 2010, Comput. Phys. Commun., 181, 380

Warwick, J. W. 1967, Space Sci. Rev., 6, 841

West, R. A., Baines, K. H., Friedson, A. J., et al. 2004, in Jupiter: The Planet, Satellites and Magnetosphere, ed. F. Bagenal, T. E. Dowling, & W. B. McKinnon (Cambridge University Press), 79–104

This 2-column preprint was prepared with the AAS LaTeX macros v5.2.